Available online at www.sciencedirect.com

SCIENCE DIRECT®

Earth and Planetary Science Letters 237 (2005) 893–910

EPSL

www.elsevier.com/locate/epsl

2-D numerical simulations of groundwater flow, heat transfer and ^{4}He transport — implications for the He terrestrial budget and the mantle helium–heat imbalance

Maria Clara Castro [a,*], Delphine Patriarche [a,1], Patrick Goblet [b,2]

[a] *University of Michigan, Department of Geological Sciences, 2534 C. C. Little Building, Ann Arbor, MI 48109-1005, United States*
[b] *Ecole des Mines de Paris, Centre d'Informatique Géologique, 77305 Fontainebleau, France*

Received 31 January 2005; received in revised form 15 May 2005; accepted 8 June 2005
Available online 9 August 2005
Editor: S. King

Abstract

Because helium and heat production results from a common source, a continental ^{4}He crustal flux of $4.65*10^{-14}$ mol m^{-2} s^{-1} has been estimated based on heat flow considerations. In addition, because the observed mantle He/heat flux ratio at the proximity of mid-ocean ridges ($6.6*10^{-14}$ mol J^{-1}) is significantly lower than the radiogenic production ratio ($1.5*10^{-12}$ mol J^{-1}), the presence of a terrestrial helium–heat imbalance was suggested. The latter could be explained by the presence of a layered mantle in which removal of He is impeded from the lower mantle [R.K. O'Nions, E.R. Oxburgh. Heat and helium in the Earth, Nature 306 (1983) 429–431; E.R. Oxburgh, R.K. O'Nions, Helium loss, tectonics, and the terrestrial heat budget, Science 237 (1987) 1583–1588]. van Keken et al. [P.E. van Keken, C.J. Ballentine, D. Porcelli, A dynamical investigation of the heat and helium imbalance, Earth Planet. Sci. Lett. 188 (2001) 421–434] have recently claimed that the helium–heat imbalance remains a robust observation. Such conclusions, however, were reached under the assumption that a steady-state regime was in place for both tracers and that their transport properties are similar at least in the upper portion of the crust. Here, through 2-D simulations of groundwater flow, heat transfer and ^{4}He transport carried out simultaneously in the Carrizo aquifer and surrounding formations in southwest Texas, we assess the legitimacy of earlier assumptions. Specifically, we show that the driving transport mechanisms for He and heat are of a fundamentally different nature for a high range of permeabilities ($k \leq 10^{-16}$ m^2) found in metamorphic and volcanic rocks at all depths in the crust. The assumption that transport properties for these two tracers are similar in the crust is thus unsound. We also show that total ^{4}He/heat flux ratios lower than radiogenic production ratios do not reflect a He deficit in the crust or mantle original reservoir. Instead, they reflect the combined impact of air saturated water (ASW), advection, conduction, and diffusion when steady-state is reached for both tracers. We thus argue that the observed low mantle He/heat flux ratio in the oceans might be, at least partially, the result of processes occurring in the oceanic crust similar to those occurring in the continental crust, rather than deeper into the mantle.

* Corresponding author. Tel.: +1 734 615 3812; fax: +1 734 763 4690.
E-mail addresses: mccastro@umich.edu (M.C. Castro), delfpat@umich.edu (D. Patriarche), patrick.goblet@ensmp.fr (P. Goblet).
[1] Tel.: +1 734 647 5732; fax: +1 734 763 4690.
[2] Tel.: +33 1 64 69 47 49; fax: +33 1 64 69 47 03.

doi:10.1016/j.epsl.2005.06.037

Our simulations also indicate that in order for both heat and He to be in steady-state in recently formed crust, the presence of an advective dominated regime is required ($k \geq 10^{-16}$ m^2). Under these conditions, only in total absence of contact with ASW (e.g., an atmospheric component provided by freshwater or seawater) is the total ^{4}He/heat flux ratio expected to equal the radiogenic production ratio. Lower ^{4}He/heat fluxes in an advective dominated regime require the incorporation of an ASW component. We argue that the observed low ocean mantle ^{4}He/heat flux results, at least partially, from sea water incorporation within mid-ocean ridge basalts. Our simulations also suggest that ^{4}He transport is in transient state in recently formed crust for permeabilities $\leq 10^{-17}$ m^2. Under these conditions, low to very low mantle He excesses and thus total He/heat fluxes of up to several orders of magnitude lower than the radiogenic production ratios are expected.

Keywords: helium–heat imbalance; ^{4}He/heat flux ratios; groundwater flow modeling; hydraulic conductivity; gulf Coast Basin

1. Introduction

The study of helium isotopes and heat flow offers a powerful tool to investigate a diversity of problems, from the deep Earth's interior to its surface, as well as the evolution of the atmosphere [4,5]. Among its numerous applications, the study of these two distinct tracers in large-scale groundwater systems can enhance our understanding of both groundwater flow [6–9], and crust and mantle dynamics through quantification of helium and heat fluxes [1,2,10–12].

He concentrations in groundwaters usually exceed those expected for water in solubility equilibrium with the atmosphere (ASW). With the exception of very shallow aquifers or recharge areas, the observed He excesses result from two main sources: a) U and Th decay in addition to ^{6}Li(n,α) ^{3}H(^{3}He) reaction giving origin to crustally produced (in-situ and deep crust) radiogenic ^{4}He and nucleogenic ^{3}He, respectively; b) mantle contributions to both ^{3}He and ^{4}He. Similarly, in old Precambrian regions, two components of heat flow are present: a) a radiogenic (crustal) component resulting from U, Th (~85%), and K (~15%) decay, and; b) a background component which originates in the mantle. In Cenozoic terrains, a cooling component might also be present [4].

Because helium and heat production results from a common source, a continental ^{4}He crustal flux of $4.65 * 10^{-14}$ mol m^{-2} s^{-1} could be estimated [1] using an estimated U content derived from continental radiogenic heat flow. Such calculation was performed under the assumption that a steady-state regime was in place for both tracers and that their transport properties are similar at least in the upper portion of the crust. In addition, based on the observed low mantle He/heat flux ($6.6 * 10^{-14}$ mol J^{-1}) at the proximity of mid-ocean ridges, it was concluded [1,2] that the amount of U and Th required to support the oceanic radiogenic He flux would only provide ~5% of the mantle heat flux. The latter is based on the presence of an oceanic crust strongly depleted in He, in addition to assumptions previously made for the continental crust. To account for this "helium–heat imbalance", the presence of a layered mantle was suggested in which removal of He is impeded from the lower mantle from which most of the heat lost through ocean basins would originate [1,2]. The terrestrial "helium–heat imbalance" problem remains unresolved at present (see, e.g., Anderson [13], van Keken et al. [3], Albarède [14], Anderson [15]).

In the last two decades, numerical simulations have become important tools to test conceptual basin-scale models of fluid migration, heat flow and reactive chemical transport [16–18]. Traditionally, such simulations were aimed at unraveling the evolution of sedimentary basins, as well as hydrocarbon and mineral deposits generation and migration. More recently, basin-scale numerical simulations of coupled water flow and He transport were conducted [10,11]. These were aimed at improving our understanding of both water dynamics and He transport in these regional systems, in addition to quantifying the magnitude of the crustal He flux. Specifically, the magnitude of the crustal ^{4}He flux determined underneath the Paris Basin [11] was found to be a factor of ~3 times greater than the ^{4}He crustal flux previously estimated by [1] based on radiogenic heat flow considerations. In order to understand the behavior of the helium–heat couple in the crust, it is necessary to simultaneously account for transport processes of these two tracers, in addition to fluid flow.

Here, through a series of simultaneous 2-D water flow–heat transfer–^{4}He transport simulations in the regional Carrizo aquifer and surrounding formations in southwestern Texas, we aim at clarifying some apparent observed thermal and He inconsistencies in continental areas (e.g., [19]), as well as to shed some light on the mantle helium–heat imbalance problem. Specifically, by analyzing the driving transport mechanisms of these two tracers, we assess the legitimacy of earlier assumptions [1,2]. The role played by advection, conduction, and diffusion on vertical transport as well as its dependency on formation permeabilities and hydraulic conductivities is analyzed. Transition from transient to steady-state regimes for heat transfer and He transport under different groundwater flow scenarios is also investigated. It will be shown that the driving transport mechanisms for heat and ^{4}He in the crust are of a fundamentally different nature. In addition, we show that the impact of ASW on both heat and He leads to significantly lower He/heat fluxes as compared to radiogenic production ratios. Our simulations indicate that, unlike heat flow, ^{4}He transport will not be at steady-state in low permeability, recently formed crust of Miocene–Pliocene–Quaternary age. Thus, and unlike O'Nions and Oxburgh [1], Oxburgh and O'Nions [2], and van Keken et al. [3], we argue that there is at present no sound basis to support the existence of a mantle helium–heat imbalance, and thus, the existence of an impermeable layer between the upper and lower mantle to He transport.

2. Geological and hydrogeological background

The Carrizo aquifer is part of a thick regressive sequence of terrigenous clastics that formed within fluvial, deltaic and marine depositional systems in the Rio Grande Embayment area of South Texas on the northwestern margin of the Gulf Coast Basin (Fig. 1a).

In Atascosa and McMullen counties (Fig. 1b), the Carrizo aquifer is a confined, massive, sandstone lying unconformably on the lower part of the upper-Wilcox and the lower-Wilcox formation (Fig. 1c; [20,21]). Downdip, the Carrizo contains an increasing amount of shales and mudstones [22,23]. The underlying lower-Wilcox, the oldest formation of Tertiary age, contains thick mudstone and clay layers. The Recklaw formation, a confining layer primarily composed of shale, fine sand and marine mudstones, conformably overlies the Carrizo aquifer and is in turn overlain by the Queen City aquifer that consists of thick coastal barrier sands in the study area. These formations outcrop subparallel to the present-day coastline as a southwest–northeast wide band across Texas; dip is to the southeast (Fig. 1a, c). The Carrizo aquifer terminates at a major 32 km wide growth-fault system commonly known as the Wilcox Geothermal Corridor (Fig. 1a, b). Groundwater flows gravitationally from the outcrop areas toward the southeast. Discharge occurs by cross-formational upward leakage along the entire formation, and along fault-related permeability pathways.

Our study area lies within the thin transitional crust, at the boundary with the thick transitional one [24]. Originally part of the Gondwanan continent, the thin transitional crust is composed of varied Precambrian and Paleozoic rocks [25].

3. Conceptual model

Coupled groundwater flow, heat transfer, and ^{4}He transport simulations were carried out simultaneously in a 2-D model encompassing four stratigraphic units, the Carrizo and overlying Queen City aquifers, and the Recklaw and upper-Wilcox confining layers (cross-section AA′, Fig. 1b, c). It is represented by a mesh corresponding to a 120.6 km long stratigraphic cross-section between 220 and −2210 meters of elevation, trending northwest–southeast (Fig. 1b, c), along the direction of regional groundwater flow. It comprises 21,939 elements. This 2-D model corresponds to the original plane from which a 3-D model comprising more than 5 million elements was constructed to carry out simulations of groundwater flow and ^{4}He transport in the region [9]. Due to today's hardware and software constraints, it is not yet possible to carry out simultaneously simulations of water flow, heat transfer, and ^{4}He transport in a 3-D model of this complexity and magnitude.

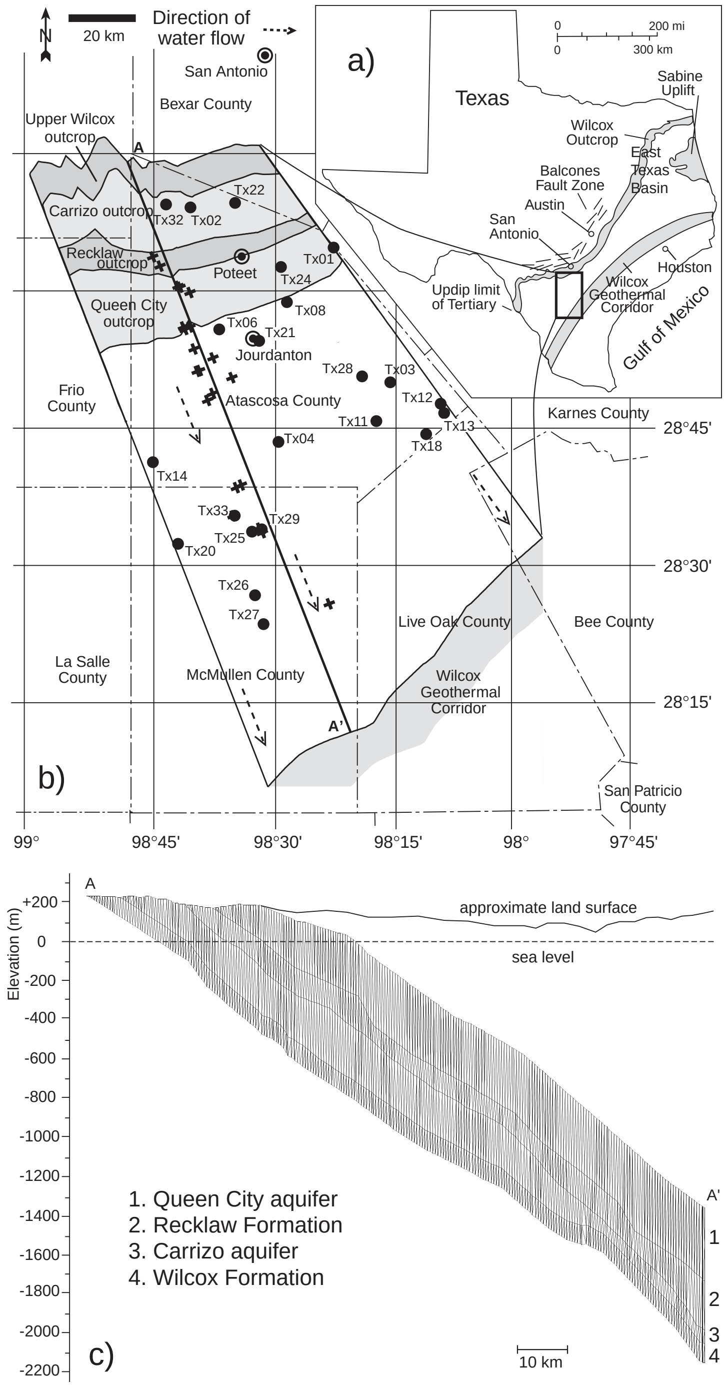

Fig. 1. a) Location and tectonic setting of the study area in southwest Texas after [21]. b) Detailed representation of the study area with location of cross-section (AA′) along which simulations were carried out; locations of water sampled for analysis of ^{4}He (closed circles) and measured temperatures are shown (crosses). c) Simplified representation of the mesh along AA′ representing the Carrizo aquifer (3) and surrounding formations; 1: Queen City aquifer, 2: Recklaw Formation, and 4: undifferentiated lower part of upper-Wilcox and lower-Wilcox.

3.1. Mathematical formulation and numerical approach

The subsurface distribution of heat in saturated porous media can be described by two coupled differential equations, one describing the fluid potential and the other temperature. We use as fluid potential an equivalent freshwater head [6] given by:

$$h = \frac{p}{\rho_0 g} + z \tag{1}$$

where p is the fluid pressure, ρ_0 an arbitrary reference density, g the gravitational constant, and z the elevation above sea level. All symbols and values used in this study are defined in Table 1.

Transient groundwater flow in response to pressure gradients is described by:

$$\nabla \cdot \left(\frac{\rho_0 g \bar{\bar{k}}}{\mu(\Theta)} \nabla h \right) = S_s \frac{\partial h}{\partial t} \tag{2}$$

with

$$\mu(\Theta) = 10^{-3} * \left(\left(0.021482 * \left(\Theta - 8.435 + \sqrt{8078.4 + (\Theta - 8.435)^2} \right) \right) - 1.2 \right)^{-1} \tag{3}$$

where μ is the dynamic viscosity, Θ is the temperature, $\bar{\bar{k}}$ is the intrinsic permeability tensor, t is time, and S_s is the specific storage coefficient. Density

Table 1
Parameters used in groundwater flow, heat transfer and ^{4}He transport simulations, and subsequent analysis

Symbol	Description	Values					Units
		Water	Queen	Recklaw	Carrizo	Wilcox	
h	Hydraulic head	computed					m
p	Fluid pressure						kg m^{-1} s^{-2}
z	Elevation above datum (sea level)						m
ρ_0	Reference water density	1000					kg m^{-3}
g	Gravitational constant	9.81					m s^{-2}
$\bar{\bar{k}}$	Permeability tensor						m^2
K	Hydraulic conductivity						m s^{-1}
Θ	Temperature	Computed					°C
Θ_0	Recharge temperature	24.7					°C
μ	Dynamic viscosity	Computed					Pa s
S_s	Specific storage coefficient		9.9E−5	9.8E−4	1.0E−4	9.8E−4	m^{-1}
$\bar{\bar{\alpha}}$	Dispersivity tensor composed of α_L and α_T						m
α_L	Longitudinal dispersivity	125					m
α_T	Transversal dispersivity	12.5					m
U	Darcy velocity	Computed					m s^{-1}
ω	Porosity		20.0	12.5	35.0	26.0	%
γ_w	Water specific heat	4.1816E+6					J m^{-3} K^{-1}
γ_{rock}	Rock specific heat		2.1E+6	2.3E+6	2.1E+6	2.3E+6	J m^{-3} K^{-1}
γ	Specific heat of the medium		2.5E+6	2.5E+6	2.8E+6	2.8E+6	J m^{-3} K^{-1}
λ_w	Water thermal conductivity	0.6					W m^{-1} K^{-1}
λ_{rock}	Rock thermal conductivity		3.5	1.2	3.5	1.2	W m^{-1} K^{-1}
λ	Thermal conductivity of the medium		2.9	1.1	2.5	1.0	W m^{-1} K^{-1}
q_{heat}	Source term of heat						W m^{-3}
q_m	Source term of mass of tracer						mol m^{-3} s^{-1}
C	^{4}He concentration	Computed					mol m^{-3}
d	^{4}He diffusion coefficient (58 °C) [8]		1.3E−9	6.7E−10	1.3E−9	6.7E−10	m^2 s^{-1}
L	Characteristic length			120			m
P_e	Peclet number						

variations are not accounted for in our simulations as the maximum combined effect of salinity and temperature on density in our domain is negligible (<1%). Because salinity effects on μ in our freshwater-dominated system are equally negligible, μ is treated as function of temperature alone.

The transient heat transfer equation accounting for advection, kinematic dispersion, and conduction is given by:

$$\nabla \cdot \left(\left(\bar{\bar{\alpha}} \gamma_w U + \lambda \right) \nabla \Theta - \gamma_w \vec{U} \Theta \right) = \gamma \frac{\partial \Theta}{\partial t} + q_{\text{heat}} \quad (4)$$

with

$$\lambda = \omega \lambda_w + (1 - \omega) \lambda_{\text{rock}} \quad (5)$$

and

$$\gamma = \omega \gamma_w + (1 - \omega) \gamma_{\text{rock}} \quad (6)$$

where $\bar{\bar{\alpha}}$ is the dispersivity tensor, λ is the thermal conductivity of the medium, λ_w and λ_{rock} are the thermal conductivities of water and the rock, respectively; γ is the specific heat of the medium, γ_w and γ_{rock} are the specific heat of the water and rock, respectively; ω is the porosity, and q_{heat} is a source term corresponding to the added (or withdrawn) heat per unit volume per unit of time.

To account for advection, kinematic dispersion, and molecular diffusion the ^4He transport equation is expressed as:

$$\nabla \cdot \left(\left(\bar{\bar{\alpha}} U + \omega d \right) \nabla C - C \vec{U} \right) = \omega \frac{\partial C}{\partial t} + q_m \quad (7)$$

where $\vec{U}$ is the Darcy velocity, d is the diffusion coefficient in porous media (diffusion coefficient in pure water multiplied by the tortuosity coefficient), C is the concentration of ^4He in water, and q_m is a source term corresponding to the added or withdrawn mass of tracer per unit volume per unit of time.

All 2-D simulations were conducted in transient state with the finite element code METIS[3] [26]. The time discretization for the resolution of the transient coupled simulations of water flow, heat transfer, and ^4He transport obeys a centered (Crank–Nicholson) scheme. The time step is automatically calculated in order to maintain the time truncation error at a fixed level.

3.2. Initial and boundary conditions

Groundwater flow boundary conditions include hydraulic heads prescribed on the outcrop areas of all formations as well as on top of the Queen City aquifer obtained using a step-by-step procedure through geostatistical modeling [9]. A no-flow boundary condition was imposed at the base of the Wilcox. In addition, a high intrinsic permeability value of $3 * 10^{-13}$ m^2 was imposed in the Wilcox Geothermal Corridor area. The latter allows for the water to be evacuated upward, translating to the situation occurring at the major growth-fault system. Intrinsic permeabilities within the Carrizo, Recklaw and Queen City Formations are our calibration parameter. In the Wilcox, to maintain a low hydraulic conductivity value [9] despite a decrease of dynamic viscosity with depth due to increased temperatures, an intrinsic permeability of 10^{-18} m^2 was imposed in the outcrop area, and a decrease factor given by $k_w = 10^{-18} \exp((z - z_w)/500)$ was applied, where z and z_w are the altitudes at the center of the elements at a location of interest, and that on the outcrop, respectively.

A temperature Θ_0 of 24.7 °C in the recharge areas of all four formations corresponding to the average of a total of 48 available measurements within the 3-D model domain recharge area was imposed [27,9]. This is the initial condition applied in all 2-D heat flow simulations. An outlet condition at the top of the confined Queen City aquifer allows heat to be evacuated upward by advection. Indeed, due to the high hydraulic conductivities (K) in place in this aquifer ($K > 2.2 * 10^{-5}$ m s^{-1}), advection is the dominant heat transport mechanism here. A heat flux representing the external heat contribution from the underlying crust and/or mantle was imposed at the base of the Carrizo aquifer; this is our heat flow calibration parameter. Inside the domain, a source term representing radiogenic in-situ heat production was imposed and calculated following [28]:

$$P_{\text{heat}} = 10^{-11} * \rho_{\text{rock}} * (9.52[\text{U}] + 2.56[\text{Th}] + 3.48[\text{K}]) \quad (8)$$

[3] Modélisation des Ecoulements et des Transferts avec Interaction en milieu Saturé.

Table 2
Th, U, and K contents in the reservoir rocks of the Queen City, Recklaw Formation, and Carrizo Aquifer as well as density and calculated ^{4}He and heat production rates

Formation	Th (ppm)	U (ppm)	K (%)	ρ_{rock} [a] (kg m^{-3})	$P^{^4He}$ (mol m$^{-3}_{rock}$ s^{-1})	P_{heat} (W m$^{-3}_{rock}$)	^{4}He/heat (mol J^{-1})
Queen[b]	6.85	2.08	1.865	2400	1.49E−18	1.05E−6	1.42E−12
Recklaw[b]	9.425	2.89	2.7	1700	1.45E−18	1.04E−6	1.40E−12
Carrizo	2.9[c]	7.50[c]	0.6702[d]	2400	3.33E−18	1.95E−6	1.71E−12

[a] Density of rocks estimated after Handbook of Physical Constants, Volume II, CRC Press, Florida, 1966.
[b] Values estimated from average lithologic composition of each formation and after Parker [29].
[c] Measured U and Th concentrations in the reservoir rock (Castro et al. [30]).
[d] Average value on 26 measurements in the Carrizo aquifer [31].

where [U], [Th] and [K] represent the U, Th, and K content of the different formations, and ρ_{rock} their respective densities (Table 2).

For the transport model an ASW ^{4}He concentration of $2.01*10^{-6}$ mol m^{-3} was imposed on all outcrop areas. This value corresponds also to the initial condition applied for all simulations. On top of the Queen City an outlet condition was prescribed, which allows ^{4}He to be evacuated upward by advection. A ^{4}He flux representing the external contribution from the underlying crust and/or mantle was imposed at the base of the Carrizo aquifer. This upward external flux is our ^{4}He transport calibration parameter. A term representing in-situ ^{4}He production (Table 2) was also imposed in the Carrizo, Recklaw and Queen City units; these were calculated using decay constants given by Steiger and Jager [32]:

$$P^{^4He} = 10^3 * \rho_{rock} * \left(1.71*10^{-25}[U] + 4.06*10^{-26}[Th]\right). \quad (9)$$

For all simulations it is assumed that in-situ produced ^{4}He is released to the water at the production rate [29].

3.3. Calibration data

Calibration of the groundwater flow model was achieved based on 34 hydraulic head measurements available in the Carrizo aquifer, located in the proximity of the 2-D model (AA′, Fig. 1b). These data belong to a total of 149 available head measurements within the 3-D model domain (AL1–8, 26–35, 37–40, 42–45, 47–48, 52, 56; SU9,10,13,14, cf. [9]).

Calibration of the heat flow model was obtained based on 21 temperature measurements available in the confined portions of the Carrizo and Queen City aquifers, in the proximity of the 2-D model (Fig. 1b, Table 3).

Calibration of the ^{4}He transport model was achieved using 11 samples located in the proximity of the 2-D model (Fig. 1b, Table 4). These are part of a total of 22 wells previously sampled in the Carrizo aquifer for analysis of noble gases ([30,33]; Fig. 1b). Previous analysis of different helium components has

Table 3
Temperature measurements [27] used for calibration of the 2–D Model

Well name	Well number	Formation	Bottom well elevation ASL* (m)	Temperature (°C)
AL001	6859401	Carrizo	41.8	26.0
AL006	7811603	Carrizo	−614.2	38.0
AL033	7803509	Carrizo	−296.3	30.0
AL034	7803507	Carrizo	−294.1	33.0
AL048	7803201	Carrizo	−129.5	29.0
AL170	6858607	Carrizo	55.2	25.0
AL189	6859804	Carrizo	−74.4	27.5
AL193	6859822	Carrizo	−73.2	28.0
AL253	7803503	Carrizo	−216.4	33.0
AL258	7803807	Carrizo	−503.5	37.0
AL319	7811604	Carrizo	−606.6	41.0
SU009	7828603	Carrizo	−1079.7	52.0
SU013	7828101	Carrizo	−1123.2	48.2
SU397	7828602	Carrizo	−1144.0	49.5
SU402	7837602	Carrizo	−1596.5	72.0
AL260	7803902	Queen City	−127.1	27.0
AL316	7811305	Queen City	−113.1	27.0
AL317	7811309	Queen City	−163.4	28.0
AL320	7812105	Queen City	−228.0	28.8
AL340	7820703	Queen City	−571.8	37.0
AL341	7820801	Queen City	−605.0	39.3

*Above sea level.

Table 4
Measured ^{4}He concentrations in the Carrizo aquifer[a]

Well name	Well number	Bottom well elevation ASL (m)	^{4}He (10^{-6} mol m^{-3})
TX 02	6851803	154.0	2.07
TX 04	7820301	−787.0	16.80
TX 06	7803601	−302.7	3.24
TX 20	7827501	−942.5	54.15
TX 21	7804803	−451.1	4.87
TX 25	7828501	−1063.5	73.06
TX 26	7836201	−1218.3	200.42
TX 27	7836902	−1330.5	265.27
TX 29	7828603	−1079.7	79.54
TX 32	6851701	140.2	1.86
TX 33	7828101	−1123.2	52.25
ASW (18 °C)[b]			2.010

[a] See Castro et al. [30]. The name, number, and bottom well elevation above sea level of well samples are indicated.
[b] After Stute et al. [33].

shown ^{4}He excesses with respect to ASW by up to two orders of magnitude (Table 4, [30]).

4. Model results and discussion

In the following sections we present and analyze simulations carried out simultaneously for groundwater flow, heat transfer and ^{4}He transport in transient state. As stated earlier, the primary goal of this study is to analyze the transport behavior of heat and ^{4}He under similar groundwater flow regimes in the crust. Therefore, emphasis will be placed on the analysis of the coupled ^{4}He-heat pair rather than at achieving a perfect fit as was previously done for ^{4}He through 3-D modeling and geostatistical analysis [9].

4.1. Groundwater, heat and ^{4}He calibrated model — ^{4}He versus heat fluxes

Simultaneous calibration on measured hydraulic heads, temperatures and ^{4}He concentrations was obtained by implementing the exponential decrease of intrinsic permeability (k) with depth in the Carrizo and Recklaw formations previously obtained through 3-D modeling [9]. This decrease results from differential compaction of the media as well as downdip lithological changes. For the Queen City aquifer where temperature measurements are also available (Table 3), an exponential decrease of k with depth was also applied, but the factor was less pronounced. These relationships are given by:

$$k_c = 5*10^{-11}\exp((z - z_c)/243.1)$$

$$k_r = 2.1*10^{-15}\exp((z - z_r)/264)$$

$$k_q = 2.5*10^{-11}\exp\left((z - z_q)/500\right) \tag{10}$$

where z_c, z_r, and z_q are the altitudes at the center of the element located on the outcrops of the Carrizo, Recklaw, and Queen City, respectively. Initial k values (outcrop areas) for the Carrizo, Recklaw, and Queen City are $5*10^{-11}$, $2.1*10^{-15}$, and $2.5*10^{-11}$ m^2, respectively. The obtained fit for calculated and measured hydraulic heads is very good, with r^2=0.98 (not shown).

Fig. 2a shows the calculated thermal field obtained through calibration of the heat flow model. Distribution of isotherms clearly shows the impact of recharge water entering the outcrop areas, which leads to a slow temperature increase and thus, low geothermal gradient (~1.3 °C/100 m) within the first ~50 km from the outcrop area. As water velocity decreases with increased recharge distance, heat accumulation in the system, due particularly to the external heat flux entering the base of the Carrizo aquifer, becomes more prominent. Irregular distribution of isotherms in the system is the combined result of downward recharge water movement, variable hydraulic gradient (steeper in the recharge area) and changes in formation dip (Fig. 1c; see also [6]). The fit obtained between calculated and measured temperatures is good (r^2=0.96, Fig. 2b). Calibration was achieved for an external heat flux entering the base of the Carrizo of 35 mW m^{-2}. If one takes into account the radiogenic heat production within our 2-D system above the base of the Carrizo (~700 m thick) as well as production in the remaining sedimentary sequence up to the surface (~1.6 km), this will correspond to an estimated surface heat flux of ~38 mW m^{-2} (Table 2).[4] Such low heat fluxes are typical of old continental and oceanic regions (Section 2; [4]).

[4] This calculation assumes a sedimentary sequence above the 2-D domain shale (50%) and sandstone (50%) dominated, with compositions represented by the Recklaw and Carrizo formations, respectively (Table 2).

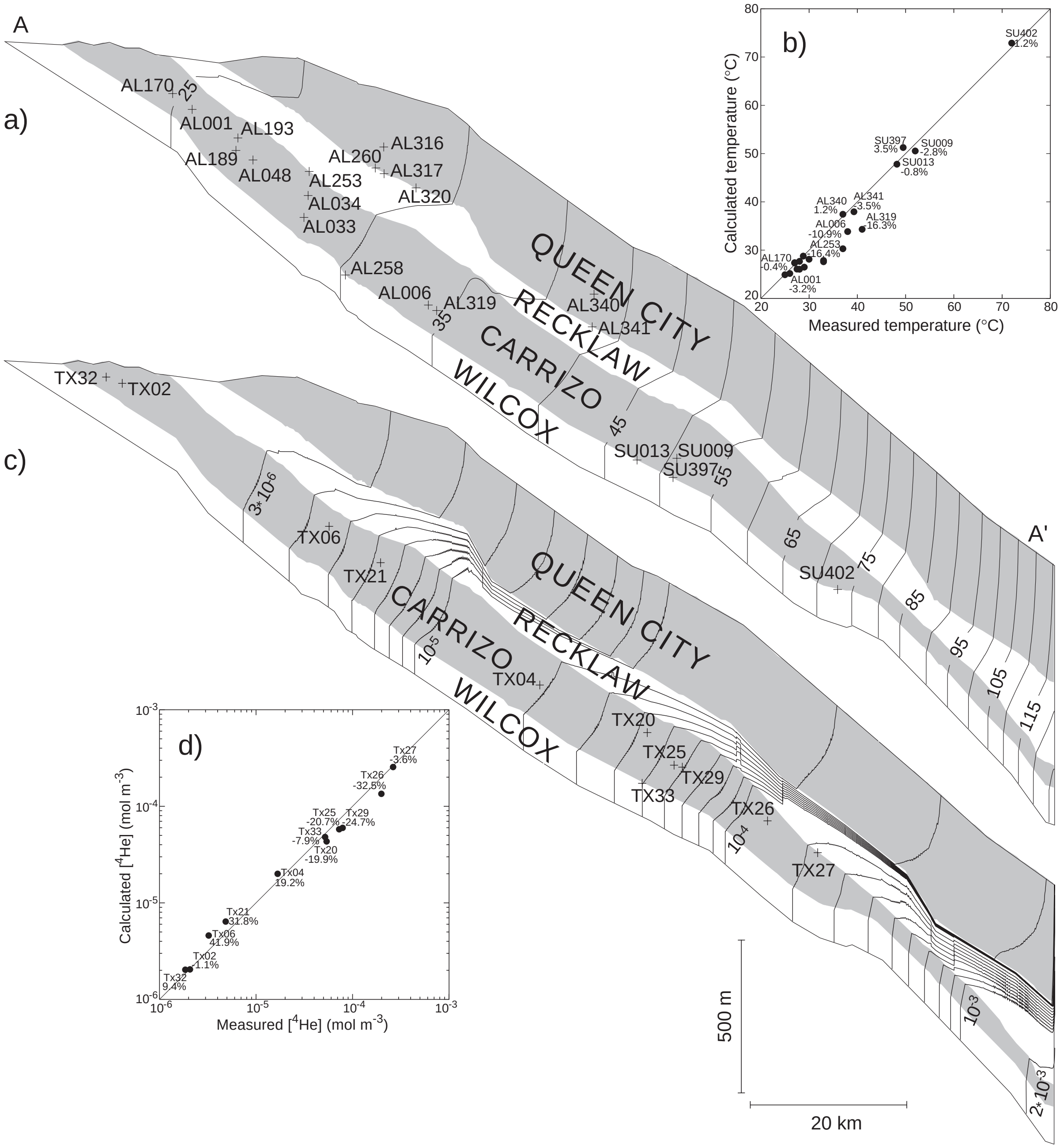

Fig. 2. a) and c) Distribution of calculated temperatures (°C) and ^{4}He concentrations (mol m^{-3}), respectively, for the calibrated reference model. Location of wells used for calibration is indicated. ^{4}He contour lines express constant variations of one unit inside each order of magnitude between $3*10^{-6}$ and $2*10^{-3}$ mol m^{-3}; b) Calculated versus measured temperature along AA′, for the reference model; line 1 : 1 is indicated; d) Calculated versus measured ^{4}He concentrations along AA′, for the reference model; line 1 : 1 is indicated.

Calibration of the ^{4}He transport model (Fig. 2c) was achieved by prescribing a flux entering the base of the Carrizo aquifer of $2.6*10^{-15}$ mol m^{-2} s^{-1}. Note that this flux is not representative of the terrestrial ^{4}He flux. Indeed, as shown by Castro et al. [10,11], ^{4}He fluxes decrease rapidly toward the surface as a result of progressive dilution by recharge water present in deeper aquifers/formations. Calculated and measured concentrations are also well correlated ($r^2=0.96$; Fig. 2d). Progressive down dip increase of ^{4}He concentrations in the Carrizo is apparent from the vertical concentration contour lines (Fig. 2c). In a similar manner to that of heat accumulation, the increase rate is slower near recharge areas where water movement is faster and the atmospheric component has a strong dilution effect on ^{4}He concentrations. In the central part of the system ^{4}He accumulates more rapidly due both to the external flux entering the Carrizo aquifer and in-situ production, as hydraulic conductivities and water velocities progressively decrease and thus, effect a smaller amount of dilution by the atmospheric component. In contrast to the Carrizo aquifer, ^{4}He concentrations persist over long distances within the Recklaw Formation because hydraulic conductivities and therefore water velocities greatly decrease with distance and depth, and are a factor of ~3 orders of magnitude smaller than those in place in the Carrizo aquifer.

This calibrated model represents one of the best fits obtained simultaneously for groundwater flow, heat transfer and ^{4}He transport models and is our "reference" in the discussion that follows. Note that small variations of both heat and ^{4}He external fluxes lead to equally good fits. Nevertheless, both heat and ^{4}He fluxes entering the base of the Carrizo are well constrained in the system within a small range of values.

It is important to note upfront that our resulting calibrated ^{4}He/heat flux ratio entering the base of the Carrizo aquifer is $7.4*10^{-14}$ mol J^{-1}, a value significantly lower than radiogenic production ratios in the area ($1.5*10^{-12}$ mol J^{-1}; Table 2), as well as that of the crust as a whole ($1.4*10^{-12}$ mol J^{-1}; Table 5). By contrast, and although at first view unrelated, it is of relevance to mention that the external ^{4}He/heat flux ratio entering the base of the Carrizo aquifer is extremely close (indistinguishable) to the mantle He/heat flux value of $6.6*10^{-14}$ mol J^{-1} reported in the oceans [1,2], at the proximity of mid-ocean ridges. The latter, which is thus also over one order of magnitude lower than the radiogenic production ratio is at the center of the so-called mantle helium–heat imbalance and the theory of a layered mantle with an impermeable boundary to He that could explain the discrepancy observed [1,2]. These apparently contradictory results raise two critical questions: a) why is the ^{4}He/heat flux ratio entering the Carrizo aquifer over one order of magnitude smaller as compared to the relatively homogeneous terrestrial radiogenic production ratio of ~10^{-12} mol J^{-1}?, and; b) is it a simple and striking coincidence that both ^{4}He/heat flux ratios entering the Carrizo aquifer and the observed oceanic mantle ratio yield indistinguishable values? Note that both observed and computed He/heat flux ratios were made either within the upper crust close to land surface (this work), or just above the crust (ocean mantle flux ratio [1,2]), rather than in the deep crust or directly in the mantle. Below, we take a closer look at possible reasons for such discrepancies.

Table 5
Th, U, and K content of the continental and oceanic crust as well as density, and ^{4}He and heat production rates

	Th (ppm)	U (ppm)	K (%)	ρ_{rock} (kg m^{-3})	P^4He (mol m$_{rock}^{-3}$ s^{-1})	P_{heat} (W m$_{rock}^{-3}$)	^{4}He/heat (mol J^{-1})
Upper crust*	10.7	2.8	2.80	2600	2.37E−18	1.66E−06	1.43E−12
Lower crust*	1.06	0.28	0.28	3300	3.00E−19	2.10E−07	1.43E−12
Oceanic crust*	0.22	0.1	0.12	3000	7.80E−20	5.80E−08	1.35E−12

Densities after Clark and Ringwood [34].
*Taylor and McLennan [35].

4.2. Sensitivity analysis to hydraulic conductivity — advective versus conductive and diffusive flow regimes

Although some similarities are observed between heat and ^4He transport at the proximity of the outcrops (Fig. 2a, c) where the influence of recharge water is strong (e.g., slow accumulation of both heat and ^4He), 2-D simulations highlighted in a clear fashion some striking behavioral differences between these two tracers. Specifically, low sensitivity of heat flow to low permeability and thus hydraulic conductivity values, by contrast to a much stronger dependency of ^4He to this same parameter and range of values.

Fig. 3a, b where temperature and ^4He concentration deviations (%) in the Carrizo aquifer are plotted for k_c and k_r values (k) 2, 5 and 10 times smaller, as well as 2, 5, and 10 fold with respect to our reference model, illustrate in a clear fashion the distinct response of these two tracers to permeability (k) and hydraulic conductivity (K) values. Specifically, scenarios $k/2$, $k/5$, and $k/10$ show in a clear fashion the independent nature of heat flow to low permeabilities and thus, hydraulic conductivities. Indeed, as k decreases with depth and thus, with distance from the outcrop, temperature deviations become very small (≤3%, ~50 km from the outcrop; Fig. 3a), to almost completely vanish at ~90 km away from the recharge area. The opposite situation is observed with ^4He concentrations (Fig. 3b), as deviations from the reference model become stronger with decreasing K, and reach a maximum of ~700% for $k/10$ simulations at ~70 km. By contrast, for k 2, 5, and 10 fold, heat flow and ^4He transport display a more similar behavior (Fig. 3a, b). Here, although ^4He deviations remain stronger, deviations increase for both tracers. Such behavior can be understood in terms of the advective/diffusive (^4He) and advective/conductive (heat) flux ratios in place in the Recklaw, the confining layer above the Carrizo aquifer where heat flow and ^4He transport are essentially vertical, upward. Indeed it has been shown [8,9] that upward ^4He movement in this 2-D system is mostly controlled by permeabilities and hydraulic conductivies in this confining layer. Dispersive flux is minor with respect to the advective, conductive and diffusive components, and thus it will not be discussed here.

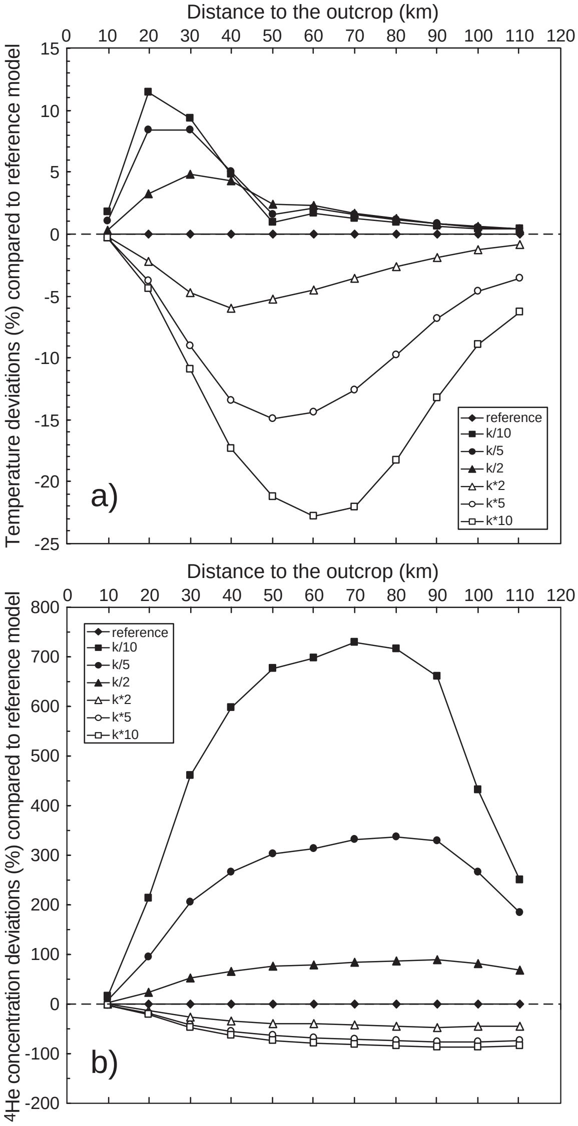

Fig. 3. a) and b) Temperature and ^4He concentration deviations (%) in the Carrizo aquifer plotted for k_c and k_r values (k) 2, 5 and 10 times smaller, as well as 2, 5, and 10 fold with respect to our reference model as a function of the distance to the Carrizo outcrop, respectively.

Advective and diffusive fluxes for ^4He and heat are given respectively by:

$$\phi_{\rm adv} = \vec{U}C \qquad \phi_{\rm adv} = \gamma_{\rm w}\vec{U}\Theta$$

$$\phi_{\rm diff} = -\omega d\frac{\delta C}{\delta z} \quad \phi_{\rm cond} = -\lambda\frac{\delta\Theta}{\delta z}. \tag{11}$$

Fig. 4 represents the ^{4}He advective/diffusive and heat advective/conductive flux ratios computed in the Recklaw as a function of distance from the outcrop (recharge distance), intrinsic permeabilities (k) and corresponding hydraulic conductivities (K). It is apparent that both ratios decrease with increasing recharge distance and decreasing K. However, while advection largely dominates transport of ^{4}He (advective/diffusive flux $\gg$ 1) throughout most of the formation, the shift from advective to conductive heat flow (advective/conductive flux $\approx$ 1) takes place at ~55 km, where K~1.5 * 10^{-9} m s^{-1}, and k~10^{-16} m^2. Conduction becomes the dominant transport mechanism (advective/conductive flux $\approx$ 0.1) for K~2.1 * 10^{-10} m s^{-1} (k=8.9 * 10^{-18} m^2) at ~90 km, entirely dominating heat flow (advective/conductive flux $\leq$ 0.01) for $K \leq$ 4.7 * 10^{-11} m s^{-1} ($k \leq$ 1.2 * 10^{-18} m^2) at a distance of ~110 km. This contrasts markedly with the dominant advective ^{4}He transport over most of the domain (Fig. 4). Only for K=4.7 * 10^{-11} m s^{-1} at ~110 km does the diffusive flux equals the advective one, and only at the very end of the 2-D domain (K=3.9 * 10^{-11} m s^{-1}; k=9.3 * 10^{-19} m^2) does the diffusive flux become dominant (advective/diffusive flux $\approx$ 0.1). Even here, the dominance of the conductive over the advective flux is stronger as compared to the diffusive versus advective flux.

Our results are similar in nature to Bickle and McKenzie [36] who, through a 1-D analysis, simulated heat and solute transport under conditions representing rocks undergoing metamorphism. These authors subdivided fluid flow regimes into three classes (page 389): "one in which advection of both heat and matter predominate, a second in which heat is largely conducted but matter is advected, and a third in which advection of both heat and matter is insignificant". Here, we find these same three classes for heat and ^{4}He transport in the Recklaw Formation for which the threshold between each class corresponds to a specific k value. Threshold between the first and second classes takes place at k~10^{-16} m^2, and threshold between the second and third classes takes place at k~10^{-18} m^2 (Fig. 4). The threshold value found in the Recklaw for advective versus conductive heat flow is

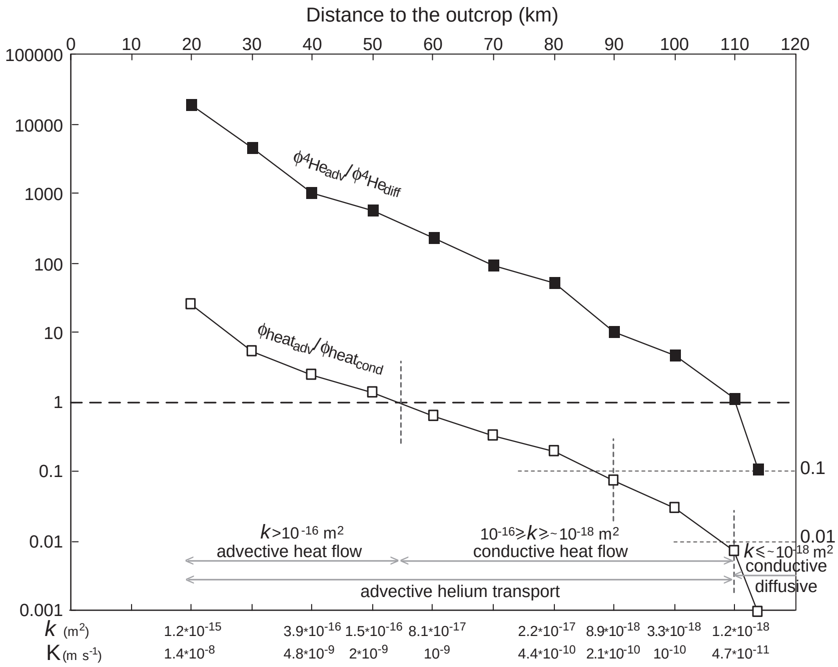

Fig. 4. ^{4}He advective/diffusive $\phi^4He_{adv}/\phi^4He_{diff}$ (closed squares), and heat advective/conductive $\phi heat_{adv}/\phi heat_{cond}$ (open squares) flux ratios computed in the Recklaw formation for our reference model as a function distance from the Carrizo outcrop (recharge distance), Recklaw intrinsic permeabilities (k), and corresponding hydraulic conductivities (K). Advective, conductive, and diffusive regimes for heat transfer and helium transport are indicated.

also in agreement with findings by Smith and Chapman [6], as well as those found in many magmatic-hydrothermal systems (see Manning and Ingebritsen [37]).

The at least two order of magnitude difference found between the permeability threshold for heat conduction ($k \sim 10^{-16}$ m^2) and ^{4}He diffusion ($k \sim 10^{-18}$ m^2) in the Recklaw Formation indicates that vertical heat flow is far more independent of low permeabilities and thus, hydraulic conductivities than ^{4}He transport. Consequently, the ability for heat to move upward within at least this permeability range values ($10^{-16} \geq k \geq 10^{-18}$ m^2) is far greater than that of ^{4}He (Fig. 4). Among geological formations that typically lie on these low hydraulic conductivity/permeability category are many igneous and metamorphic rocks (e.g., granites, basalts, gneiss, see [37]) both in the near-surface and deep crust. We now analyze the implications of these findings on the observed ^{4}He/heat flux ratios.

4.3. Impact of ASW, diffusion and conduction on observed ^{4}He/heat flux ratios

Fig. 5 represents the advective ^{4}He/heat, ^{4}He diffusive/heat conductive, and the total ^{4}He/heat vertical flux ratios computed in the Recklaw Formation with respect to distance from the outcrop, and permeabilities (k). Total ^{4}He/heat flux remains unchanged with or without dispersive flux. The following is apparent: a) Advective ^{4}He/heat flux ratios are much lower than radiogenic crustal production ratios (1.4–$1.5 * 10^{-12}$ mol J^{-1}) at the proximity of the outcrop area ($2.5 * 10^{-14}$ mol J^{-1}, ~20 km; $k = 1.2 * 10^{-15}$ m^2). Here advection is the main transport mechanism for both ^{4}He and heat and advective ^{4}He/heat flux ratio equals that of total ^{4}He/heat flux. Low flux ratios are the result of ASW dilution exerted by recharge water (atmospheric component) on ^{4}He concentrations as opposed to its much smaller impact on the thermal field (see Section 4.2, Fig. 3a, b). The

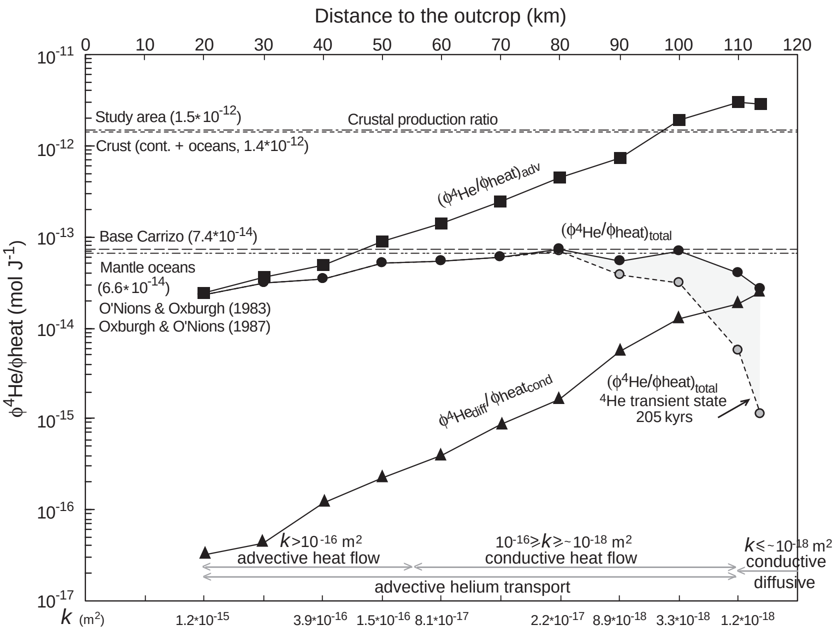

Fig. 5. Steady-state advective ^{4}He/heat (ϕ^4He/ϕheat)$_{adv}$ (closed squares, solid line), ^{4}He diffusive/heat conductive (ϕ^4He$_{diff}$/ϕheat$_{cond}$) (closed triangles, solid line), and total ^{4}He/heat (ϕ^4He/ϕheat)$_{total}$ (closed black circles, solid line) vertical flux ratios computed in the Recklaw Formation with respect to the distance from the Carrizo outcrop, and permeabilities (k). Crustal radiogenic production ratios for the study area ($1.5 * 10^{-12}$ mol J^{-1}; Table 2) as well as for the crust ($1.4 * 10^{-12}$ mol J^{-1}; Table 5) are indicated. External total ^{4}He/heat flux entering the base of the Carrizo ($7.4 * 10^{-14}$ mol J^{-1}), and that observed at the proximity of the ocean ridges [1,2] are indicated ($6.6 * 10^{-14}$ mol J^{-1}). Total ^{4}He/heat fluxes are also indicated for ^{4}He transient state transport and heat flow steady-state at ~205 kyrs (dashed line, closed gray circles). Low total ^{4}He/heat fluxes observed for transient ^{4}He transport while under a steady-state heat flow regime are also indicated (gray area).

greater impact of ASW on He as compared to heat in an advective dominated regime such as the recharge area can be understood in terms of the respective diffusive (He) and thermal (heat) Peclet numbers, given respectively by [38]:

$$P_{e_{\mathrm{diffusive}}} = \frac{UL}{\omega d} \quad P_{e_{\mathrm{thermal}}} = \frac{\gamma_{\mathrm{w}} UL}{\lambda} \tag{12}$$

where L is a characteristic length of the porous media (thickness of the Recklaw Formation, for example). If both Peclet numbers are $\gg 1$ both heat and He advective fluxes entirely dominate with respect to the conductive and diffusive fluxes. At the proximity of the recharge area, however, where the Darcy velocity is ~$2.4*10^{-9}$ ms^{-1} and L~120 m, the diffusive Peclet number is much greater (~3460) than the thermal one (~1.1). Thus, while advection entirely dominates over diffusion, thermal conduction plays a non-negligible role with respect to advection. This greater dominance of advection over diffusion as compared to conduction in the recharge area is precisely at the origin of the greater ASW impact on He concentrations as compared to temperatures and translates directly into a much greater diffusive Peclet number as compared to the thermal one. As impact of ASW decreases due to permeability and hydraulic conductivity decrease, advective ^{4}He/heat flux ratios increase steadily by up to about two orders of magnitude to approach radiogenic production values only when the impact of ASW water (not shown) on both tracers is negligible (<1%), with $k \leq 3.3*10^{-18}$ m^2 (100–110 km). Transport by advection however, is insignificant in this area (Fig. 5); b) In contrast to advection, diffusion and conduction play a negligible role on ^{4}He and heat transport at the proximity of the outcrop (~20 km; Figs. 4 and 5) and ^{4}He diffusive/heat conductive flux ratios display extremely small values in this area ($7.8*10^{-17}$ mol J^{-1}, Fig. 5). A stronger ^{4}He concentration than temperature gradient increase leads to a steady increase of this ratio with permeability and hydraulic conductivity decrease, of up to $2.4*10^{-14}$ mol J^{-1} (113.75 km; $k=9.3*10^{-19}$ m^2). Here, transport by diffusion and conduction is dominant and ^{4}He diffusive/heat conductive flux equals that of total ^{4}He/heat flux ratios.

It can also be seen that although advective ^{4}He/heat and diffusive ^{4}He/conductive heat fluxes vary over several orders of magnitude, total ^{4}He/heat flux ratios vary within a relatively narrow range (~2.4–$7.8*10^{-14}$ mol J^{-1}) despite a 4 order of magnitude permeability variation within the Recklaw Formation alone (Fig. 5). While total ^{4}He/heat flux ratios remain consistently below the radiogenic production ratio, such low values do not reflect a He deficit in the original reservoir where they originate (deeper crust or mantle). Instead, they reflect the combined impact of ASW (atmospheric component), advection, conduction, and diffusion on these two tracers. The interplay between these different components and the extent to which each one influences this ratio depends in turn on permeabilities and therefore, hydraulic conductivities of the formations they cross in their movement upward, toward the surface. Our results show that only in the total absence of contact with ASW (e.g., an atmospheric component provided by freshwater or seawater) under an advective dominated regime for both ^{4}He and heat transport is the total ^{4}He/heat flux ratio expected to equal the radiogenic production ratio. In the field, and although unlikely, this situation could hypothetically be found on a deep high permeability fault where $k \geq 10^{-16}$ m^2.

It is important to note that although our simulations ran in transient state, all results presented here correspond to the field situation once steady-state has been reached for groundwater flow, heat and ^{4}He transport. The distinct nature of heat flow and ^{4}He transport in low permeability formations ($k \leq 10^{-16}$ m^2) has also a major impact on the presence of transient versus steady-state transport for both tracers. This, in turn, has also major implications on the observed ^{4}He/heat flux ratios in the field. We discuss these below.

4.4. Transient versus steady-state regime for heat flow and ^{4}He transport: implications for ^{4}He/heat flux ratios

While steady-state for heat flow is reached at ~205 kyrs in our reference calibrated model (Section 4.1), that of ^{4}He transport is reached much later, at ~2.75 Myrs, i.e., a time decoupling factor of 13.4 between both tracers. Because we did not simulate the evolution of the entire sedimentary sequence, time at which steady-state for both tracers is reached in our simulations does not correspond to the real time at which steady-state was reached in the field. This is, however, irrelevant to the present goal of our study. Of relevance is the deep decoupling in time and space displayed between these two tracers under certain initial and boundary conditions within similar geological and hydrogeological contexts. Such decoupling is controlled by the permeabilities and hydraulic conductivities of the formations in place, and relates also directly to the thermal and helium diffusivities in areas in which conduction and diffusion are the dominant transport mechanisms of these two tracers. If one considers a simple monodimensional analysis thus, neglecting effects in place in a real 2- or 3-D system such as those resulting from cross-formational flow, decoupling of heat and He can be investigated by looking at the diffusivity ratio (dimensionless) of these two tracers given by:

$$\frac{\text{thermal diffusivity}}{\text{helium diffusivity}} = \frac{\lambda/\gamma}{d}. \tag{13}$$

Estimation of the diffusivity ratio for the Recklaw Formation (Table 1) yields a value of ~662. Thus, if advection were to be negligible over the entire domain, and heat and He transport by conduction and diffusion were entirely dominant, a time decoupling factor of ~662 between these two tracers would be observed. Advection, however, the dominant transport mechanism for He over most of the domain's extent (e.g., Fig. 4), greatly reduces the observed decoupling factor in our reference model (~13). Sensitivity tests have shown that as hydraulic conductivities increase (e.g., Fig. 3a, b), thus enhancing the role of advection for both tracers, decoupling between these two tracers greatly decreases. Indeed, steady-state is reached simultaneously for both tracers in areas where $k \geq 10^{-16}$ m^2 (Fig. 6), i.e., in areas where transport is dominated by advection. By contrast, time decoupling between these tracers increases as k decreases. Fig. 6 shows the percentage of ^{4}He concentrations at ~205 kyrs (heat flow steady-state) with respect to total ^{4}He concentrations at ~2.75 Myrs (^{4}He steady-state transport) as a function of distance from the outcrop area and permeabilities. The latter illustrates space decoupling in a clear fashion. Specifically, decoupling of ^{4}He becomes particularly strong at ~90 km for k~10^{-17} m^2 (~92%), and increases steeply with k decrease, to reach only ~7% of total ^{4}He at 113.75 km ($k = 9.3 * 10^{-19}$ m^2). As k further decreases, the

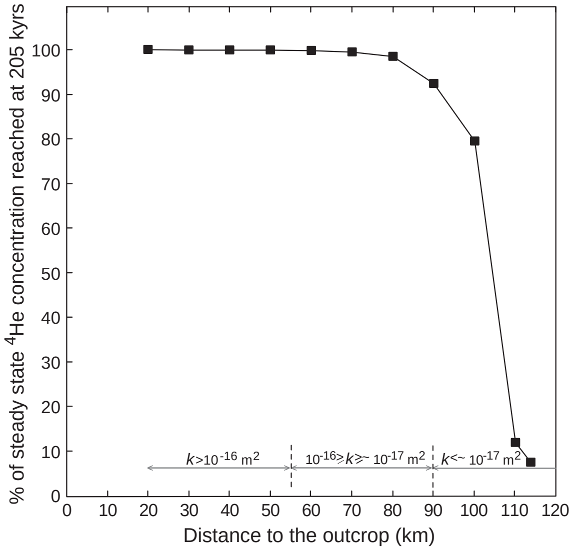

Fig. 6. Percentage of ^{4}He concentrations at ~205 kyrs (heat flow steady-state) with respect to total ^{4}He concentrations at ~2.75 Myrs (^{4}He steady-state transport) as a function of distance from the Carrizo outcrop area and permeabilities (k).

time decoupling factor between these two tracers increases. For example, heat and ^{4}He are decoupled by a time factor of 30 in scenario $k/10$ (see Section 4.2), with steady-state for heat and ^{4}He reached at ~430 kyrs and ~13 Myrs, respectively.

Absence of ^{4}He transport steady-state directly impacts total ^{4}He/heat fluxes. Indeed, while steady-sate for heat flow is in place at ~205 kyrs (reference model) and heat fluxes remain unchanged, ^{4}He fluxes are much lower in areas with $10^{-17} \geq k \geq 9.3 * 10^{-19}$ m^2 leading to total ^{4}He/heat fluxes of over an order of magnitude smaller (dashed line, Fig. 5) than those corresponding to steady-state for both tracers (solid line, Fig. 5). Thus, total ^{4}He/heat flux values as low as 10^{-15} mol J^{-1} can be found in the presence of ^{4}He transient state (~205 kyrs–2.75 Myrs) under this particular scenario.

Because many igneous and metamorphic formations display $k < 10^{-17}$ m^2, this steep time decoupling directly impacts ^{4}He/heat flux ratios in areas of recent (Miocene, Pliocene, Quaternary) magmatic or volcanic activity. Indeed, with the exception of fault areas where transport is by advection ($k \geq 10^{-16}$ m^2), positive thermal anomalies might be observed while in total absence (or slight presence) of a mantle He component in such areas. For example, heat and helium patterns observed in the central European Rhine Graben (e.g., [19]) might be the result of such temporal decoupling. By contrast, areas in which magmatic chambers that cooled at earlier times are located might give rise to observed positive mantle He anomalies while in the total absence of thermal anomalies.

4.5. Low ^{4}He/heat flux ratios — implications for the terrestrial He budget and the mantle helium–heat imbalance

Two decades ago, based on the observed low mantle He/heat flux value of $6.6*10^{-14}$ mol J^{-1} at the proximity of mid-ocean ridges [1,2] concluded that the amount of U and Th required to support the oceanic radiogenic He flux would only provide ~5% of the mantle heat flux. This low He/heat flux ratio is at the origin of the mantle helium–heat imbalance and the theory of a layered mantle with an impermeable boundary to He that could explain the discrepancy observed [1,2]. Recently, van Keken et al. [3] claimed once again that the mantle helium–heat imbalance remains a robust observation. However, the assumptions behind their study were similar to those adopted by [1,2], i.e., similar transport efficiencies for He and heat transport in the crust in addition to the presence of a steady-state transport regime. These authors thus conclude (page 423): "Therefore, the issue of separation of heat from helium centers only on the mantle fluxes".

We have shown that transport of ^{4}He and heat is of a different nature for a high range of permeability values ($k \leq 10^{-16}$ m^2) found in metamorphic and igneous rocks at all depths in the crust [37]. Consequently, the assumption behind the continental ^{4}He crustal flux estimation by [1] based on similar transport properties of both heat and He in the crust is invalidated. We have also shown that total ^{4}He/heat flux ratios lower than radiogenic production ratios do not reflect a He deficit in the original reservoir (deep crust or mantle) as compared to heat. Instead, they reflect the combined impact of ASW, advection, conduction, and diffusion when steady-state is reached for both tracers in addition to the presence of a possible transient state regime for He transport alone (Fig. 5). We thus argue that the observed low mantle He/heat flux ratio observed in the oceans (see Table 5, Fig. 5) might be, at least partially, the result of processes occurring in the oceanic crust similar to those occurring in the continental crust, rather than deeper into the mantle.

Our simulations indicate that in order for both heat and He to be in steady-state in recently formed crust, the presence of an advective dominated regime is required ($k \geq 10^{-16}$ m^2, Fig. 6, Section 4.4). Under these conditions, only in total absence of contact with ASW (e.g., an atmospheric component provided by seawater) is the total ^{4}He/heat flux ratio expected to equal the radiogenic production ratio ($1.5*10^{-12}$ mol J^{-1}, Fig. 5). Lower ^{4}He/heat flux ratios in an advective dominated regime require the incorporation of an ASW component. We thus argue that the observed low ocean mantle ^{4}He/heat flux [1,2] results, at least partially, from sea water incorporation within mid-ocean ridge basalts (MORB). Our findings are strongly supported by noble gas data from a number of MORB glasses for which Fisher [39] concluded that only the presence of variable but non-zero amounts of atmospheric/hydrospheric noble gases can explain the measured He, Ar, and Xe in a coherent manner.

Our simulations also suggest that ^{4}He transport is in transient state in recently formed crust for $k \leq 10^{-17}$ m^2 (Fig. 6), i.e., likely in most active sea-floor spreading centers. Under these conditions, low to very low mantle He excesses and thus total He/heat fluxes up to several orders of magnitude lower than the radiogenic production ratios are likely to be observed (e.g., Fig. 5, gray area). These findings are also supported by direct field observations. Indeed, the mantle He/heat flux ratio reported by [1,2] as representative of the Earth's mantle comes from one single spreading center, the East Pacific Rise, from samples collected at the triple-junction of the Pacific, Cocos and Nazca Plate by Craig et al. [40]. These authors point out that much smaller mantle He anomalies were found in the Atlantic, and that no maximum ^{3}He/^{4}He ratio anomalies could be identified in the South Pacific. It is also of interest to note the contrast between observed ^{4}He/^{40}Ar ratios in basalts from the Mid-Atlantic Ridge (MAR) and those from the East Pacific Rise (EPR) [39]. While the first are consistently greater than mean radiogenic production ratios, EPR ^{4}He/^{40}Ar ratios are, for the most part, close to the mean radiogenic production value. Comparable ^{4}He/^{40}Ar values to those of MAR were also found in the Paris Basin [10,11]. Such decoupling between ^{4}He and ^{40}Ar is due to preferential transport by diffusion of ^4He in a low permeability formation (k~$4*10^{-19}$ m^2). Decoupling of $^4He/^{40}Ar$ in the MAR thus suggests the presence of a low permeability oceanic crust in the area, and thus, the presence of transient state for ^4He transport as opposed to a potential ^4He steady-state in a more permeable EPR crust.

5. Summary

Simulations of groundwater flow, heat transfer and ^4He transport were conducted simultaneously in the Carrizo aquifer and surrounding formations in southwest Texas. Results indicate that the driving transport mechanisms for He and heat are of a fundamentally different nature in the crust, thus rendering assumptions made by O'Nions and Oxburgh [1] and Oxburgh and O'Nions [2] for estimation of the terrestrial crustal ^4He flux based on heat considerations unsound.

It is shown that ^4He/heat flux ratios below the radiogenic production ratio do not reflect a He deficit in the original reservoir where they originate (deeper crust or mantle). Instead, they reflect the combined impact of ASW, advection, conduction, and diffusion on these two tracers. The interplay between these different components and the extent to which each one influences this ratio depends on permeabilities and therefore, hydraulic conductivities of the formations they cross in their movement toward the surface. Our results show that only in total absence of contact with ASW (e.g., an atmospheric component provided by freshwater or seawater) under an advective dominated regime for both ^4He and heat transport is the total ^4He/heat flux ratio expected to equal the radiogenic production ratio. Our simulations also suggest that ^4He transport is in transient state in recently formed low permeability crust leading to low He/heat flux ratios in these formations.

Low mantle He/heat flux ratios reported at the proximity of mid-ocean ridges might be, at least partially, the result of processes occurring in the oceanic crust similar to those occurring in the continental crust, rather than deeper into the mantle. Overall, and without consideration for additional processes that might affect these two tracers in the mantle (e.g., Albarède [14], Anderson [15]), our simulations show that there is at present no scientific basis to support the existence of a mantle helium–heat imbalance and consequently, the presence of a layered mantle in which removal of He is impeded from the lower mantle [1,2]. Anderson [13,41] has previously suggested that both He and CO_2 may be trapped in the shallow mantle, a hypothesis that is consistent with our simulation results for low permeability and hydraulic conductivity formations. Alternative mantle structures and convection models are possible for which the presence of a deep impermeable boundary to He is not required (see e.g., Albarède [14], Anderson [15]).

Acknowledgments

The authors thank F. Albarède and D.L. Anderson for their constructive comments which lead to a much improved final version of this manuscript. The authors also thank S. King for the editorial handling of this manuscript. Financial support by the U.S. National Science Foundation grant EAR-03087 07, the Elizabeth Caroline Crosby Research Award (NSF ADVANCE at the University of Michigan), and the "Ministère des Affaires Etrangères", France, for D. Patriarche through the program "Bourse Lavoisier", is greatly appreciated.

References

[1] R.K. O'Nions, E.R. Oxburgh, Heat and helium in the Earth, Nature 306 (1983) 429–431.
[2] E.R. Oxburgh, R.K. O'Nions, Helium loss, tectonics, and the terrestrial heat budget, Science 237 (1987) 1583–1588.
[3] P.E. van Keken, C.J. Ballentine, D. Porcelli, A dynamical investigation of the heat and helium imbalance, Earth Planet. Sci. Lett. 188 (2001) 421–434.
[4] H.N. Pollack, The heat flow from the earth: a review, in: P.A. Davies, S.K. Runcorn (Eds.), Mechanisms of Continental Drift and Plate Tectonics, Academic Press, London, 1980, pp. 183–192.
[5] M. Ozima, F.A. Podosek, Noble Gas Geochemistry, Cambridge University Press, New York, 2002, 286 pp.
[6] L. Smith, D.S. Chapman, On the thermal effects of groundwater-flow: 1. Regional scale systems, J. Geophys. Res. 88 (B1) (1983) 593–608.
[7] D. Deming, Regional permeability estimates from investigations of coupled heat and groundwater-flow, North Slope of Alaska, J. Geophys. Res. 98 (B9) (1993) 16271–16286.
[8] M.C. Castro, P. Goblet, Calibration of regional groundwater flow models — working toward a better understanding of site-

specific systems, Water Resour. Res. 39 (6) (2003) 1172, doi:10.1029/2002WR001653.
[9] D. Patriarche, M.C. Castro, P. Goblet, Large-scale hydraulic conductivities inferred from three-dimensional groundwater flow and ^{4}He transport modeling in the Carrizo aquifer, Texas, J. Geophys. Res. 109 (2004) B11202, doi:10.1029/2004JB003173.
[10] M.C. Castro, A. Jambon, G. de Marsily, P. Schlosser, Noble gases as natural tracers of water circulation in the Paris Basin: 1. Measurements and discussion of their origin and mechanisms of vertical transport in the basin, Water Resour. Res. 34 (10) (1998) 2443–2466.
[11] M.C. Castro, P. Goblet, E. Ledoux, S. Violette, G. de Marsily, Noble gases as natural tracers of water circulation in the Paris Basin: 2. Calibration of a groundwater flow model using noble gas isotope data, Water Resour. Res. 34 (10) (1998) 2467–2483.
[12] M.C. Castro, Helium sources in passive margin aquifers — new evidence for a significant mantle ^{3}He source in aquifers with unexpectedly low in-situ ^{3}He/^{4}He production, Earth Planet. Sci. Lett. 222 (2004) 897–913.
[13] D.L. Anderson, A model to explain the various paradoxes associated with mantle noble gas geochemistry, Proc. Natl. Acad. Sci. U. S. A. 95 (1998) 9087–9092.
[14] F. Albarède, The survival of mantle geochemical heterogeneities, AGU Monograph, in press.
[15] D.L. Anderson, Self-gravity, Self-consistency and Self-organization in Geodynamics and Geochemistry, AGU Monograph Series, in press.
[16] G. Garven, R.A. Freeze, Theoretical analysis of the role of groundwater flow in the genesis of strata bound ore deposits 1. Mathematical and numerical model, Am. J. Sci. 284 (1984) 1085–1124.
[17] G. Garven, Continental-scale groundwater flow and geologic processes, Annu. Rev. Earth Planet. Sci. 23 (1995) 89–117.
[18] M. Person, J.P. Raffensperger, S.M. Ge, G. Garven, Basin-scale hydrogeologic modeling, Rev. Geophys. 34 (1) (1996) 61–87.
[19] C. Clauser, E. Griesshaber, H.J. Neugebauer, Decoupled thermal and mantle helium anomalies: implications for the transport regime in continental rift zones, J. Geophys. Res. 107 (B11) (2002) 2269, doi:10.1029/2001JB000675.
[20] D.G. Bebout, V.J. Gavenda, A.R. Gregory, Geothermal Resources, Wilcox Group, Texas Gulf Coast, Bur. Econ. Geol., Univ. Texas, Austin, 1978, 82 pp.
[21] H.S. Hamlin, Depositional and groundwater flow systems of the Carrizo–Upper Wilcox, South Texas, Bur. Econ. Geol, Rep. of Invest., vol. 175, 61 pp.
[22] H.B. Harris, Groundwater resources of LaSalle and McMullen Counties, Texas, Texas Water Development Board Bulletin, vol. 6520, 1965, 9 pp.
[23] W.H. Alexander, D.E. White, Groundwater resources of Atascosa and Frio Counties, Rep., vol. 32, Texas Water Development Board, Texas, 1966, 211 pp.
[24] D.S. Sawyer, R.T. Buffler, R.H. Jr. Pilger, The crust under the Gulf of Mexico Basin, The Geology of North America, vol. J, The Gulf of Mexico Basin, Geol. Soc. Am. (1991) 53–72.
[25] W.R. Dickinson, T.F. Lawton, Carboniferous to Cretaceous assembly and fragmentation of Mexico, GSA Bull. 113 (9) (2001) 1142–1160.
[26] P. Goblet, Programme METIS: Simulation d'écoulement et de Transport Miscible en Milieu Poreux et Fracturé – Notice de conception – Mise à jour au 1er/11/99, 1999 (Rapport CIG/LHM/RD/99/38).
[27] Texas Water Development Board, Ground-Water Database, Texas Water Development Board, 2003 (http://www.twdb.state.tx.us/publications/reports/GroundWaterReports/GWDatabaseReports/GWdatabaserpt.htm).
[28] L. Rybach, L. Stegena, R. Haenel, Determination of heat production rate, in: R. Haenel, L. Rybach, L. Stegena (Eds.), Handbook of Terrestrial Heat-Flow Density Determination, Kluwer Academic Publishers, Dordrecht, 1988, pp. 125–142.
[29] R.L. Parker, Composition of the Earth's crust, Data of Geochemistry, 6th edition. U.S. Geological Survey Professional Paper, 1967, pp. 1–19, Chapter D, U.S.G.S. 0440-D.
[30] M.C. Castro, M. Stute, P. Schlosser, Comparison of ^{4}He and ^{14}C ages in simple aquifer systems: implications for groundwater flow and chronologies, Appl. Geochem. 15 (2000) 1137–1167.
[31] S.M. Smith, National Geochemical Database: Reformatted data from the National Uranium Resource Evaluation (NURE) Hydrogeochemical and Stream Sediment Reconnaissance (HSSR) Program, Version 1.30, Open-File Report 97–492, U.S. Geological Survey, 2001 (WWW release only: http://greenwood.cr.usgs.gov/pub/open-file-reports/ofr-97-0492/index.html).
[32] R.H. Steiger, E. Jager, Subcomission on geochronology: convention on the use of decay constant in gas and cosmochronology, Earth Planet, Sci. Lett. 36 (1977) 359–362.
[33] M. Stute, P. Schlosser, J.F. Clark, W.S. Broecker, Paleotemperatures in the southwestern United States derived from noble gas measurements in groundwater, Science 256 (1992) 1000–1003.
[34] S.P. Clark Jr., A.E. Ringwood, Density distribution and constitution of the mantle, Rev. Geophys. 2 (1964) 35–88.
[35] S.R. Taylor, S.M. McLennan, The Continental Crust: Its Composition and Evolution: Blackwell Scientific, Mass, Oxford, 1985, 312 pp.
[36] M.J. Bickle, D. McKenzie, The transport of heat and matter by fluids during metamorphism, Contrib. Mineral Petrol. 95 (1987) 384–392.
[37] C.E. Manning, S.E. Ingebritsen, Permeability of the continental crust: implications of geothermal data and metamorphic systems, Rev. Geophys. 37 (1) (1999) 127–150.
[38] G. de Marsily, Quantitative Hydrogeology, Academic Press, London, 1986, 440 pp.
[39] D.E. Fisher, Rare gas abundances in MORB, Geochim. Cosmochim. Acta 50 (1986) 2531–2541.
[40] H. Craig, W.B. Clarke, M.A. Beg, Excess ^{3}He in deep water on the East Pacific Rise, Earth Planet. Sci. Lett. 26 (1975) 125–132.
[41] D.L. Anderson, A theory of the Earth: Hutton and Humpty-Dumpty and Holmes, in: G.Y. Craig, J.H. Hull (Eds.), James Hutton — Present and Future, Special Publications, vol. 150, Geological Society, London, 1999, pp. 13–35.